

Nanomechanical hydrogen sensing

X. M. H. Huang, M. Manolidis, Seong Chan Jun, and J. Hone^{a)}

*Department of Mechanical Engineering and Nanoscale Science and Engineering Center,
Columbia University, 500 W. 120th Street, New York, New York 10027*

(Received 21 December 2004; accepted 3 March 2005; published online 28 March 2005)

A nanomechanical beam resonator is used as a sensitive, specific hydrogen sensor. The beam is fabricated from AuPd alloy and tested by magnetomotive transduction at room temperature. The fundamental resonance frequency decreases significantly and reversibly at hydrogen pressures above 10^{-5} Torr, whereas the frequency shifts observed for other gases are significantly smaller. The large frequency shift is likely due to the formation of interstitial hydrogen in the metal alloy lattice, which relieves the built-in tensile stress in the resonator beam. The uptake of hydrogen as measured by frequency shift is consistent with previous studies. © 2005 American Institute of Physics. [DOI: 10.1063/1.1897445]

Nanoelectromechanical systems (NEMS) show great promise as highly sensitive detectors of mass, charge, and spin, due to their small size, high frequency, and high resonant quality factors.¹ For many applications, it would be advantageous to combine chemical specificity with the high sensitivity attainable using NEMS. Such a combination has been achieved in microscale devices,² but has not yet been reported for NEMS. Here we describe the specific sensing of hydrogen using a nanomechanical resonant beam composed of a gold–palladium alloy. Intercalation of hydrogen into the metal lattice changes the tension in the device and strongly shifts the resonant frequency.

Hydrogen sensors are important for a number of applications, and compact hydrogen sensors will become increasingly prevalent if hydrogen begins to supplant hydrocarbons as a common fuel. Nanoscale sensing elements have the advantage of rapid response and potentially high sensitivity, and recent publications have demonstrated hydrogen sensing using Pd nanowires,³ titania nanotubes,⁴ and carbon nanotubes.⁵ NEMS sensors may be able to exceed the performance of existing macro- and nanosensors in both speed and sensitivity. NEMS devices may also be useful for the study of the surface dissociation of H₂ and subsequent formation of interstitial hydrogen in a metal alloy lattice. This process is of fundamental importance, both for basic research and for industrial applications.⁶ It can play a key role in corrosion, hydrogen storage in metals, and heterogeneous catalysis. NEMS permit the study of this phenomenon at very low hydrogen concentrations, using a simple bench top apparatus.

Figure 1 shows scanning electron microscope (SEM) images of the beams used in the study. Two beams, with thickness 30 nm, width 100 nm, and lengths of 7 and 8 μm , respectively, are patterned in a resistance-bridge configuration on a Si substrate. The beams were defined using electron-beam lithography and evaporation of Au_{0.6}Pd_{0.4} alloy, followed by liftoff. We note that the choice of alloy over pure Pd is due to the smaller grain size of the alloy: pure Pd beams showed much lower resonant quality factors. The beams were then released by etching the underlying Si substrate using an isotropic CF₄/O₂ RIE process (gas pressure 250 mTorr, 300 W, rf power). The etch rate for metal in this

RIE process is negligibly small (<1 nm/min), compared to the isotropic etch rate of silicon (~ 250 nm/min). The slight bending of the suspended edge of the support structure for the resonator beams indicates that the beams are under tensile stress.

The beam resonance is detected using a magnetomotive resistance bridge technique^{7,8} [Fig. 2(a)]. The beams are placed in a vacuum chamber with a magnetic field of ~ 0.9 T in the out-of-plane direction. The field is generated by a Nd-FeB permanent magnet, allowing the entire apparatus to run on a bench top without the cryogenic equipment necessary for higher-field magnets. The output of a network analyzer (HP 3577A) is passed through a 180° power splitter to drive the beams out of phase, so that the potential of the center pad is initially virtual ground. When the drive frequency is swept to match the fundamental resonance frequency of one of the beams, resonant motion is induced, and the resulting EMF voltage is then detected. An impedance matching transformer is used to optimize signal power transfer from the device output to the input of the radio frequency amplifier. Typical mechanical resonance traces of the device are shown in Fig. 2(b), with a driving voltage of 450 μV .

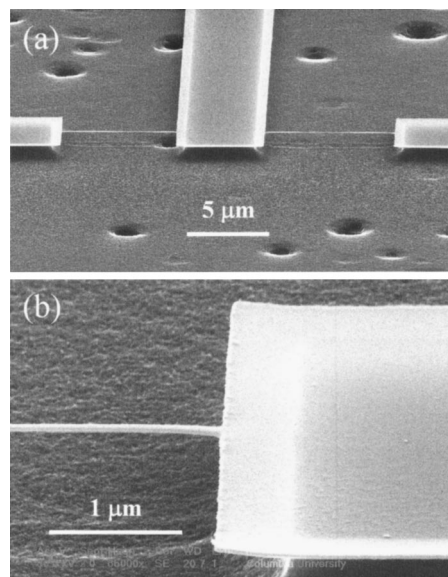


FIG. 1. SEM micrographs of the device. The zoom-in view of clamping region reveals that the metal components are under tensile stress.

^{a)}Electronic mail: jh2228@columbia.edu

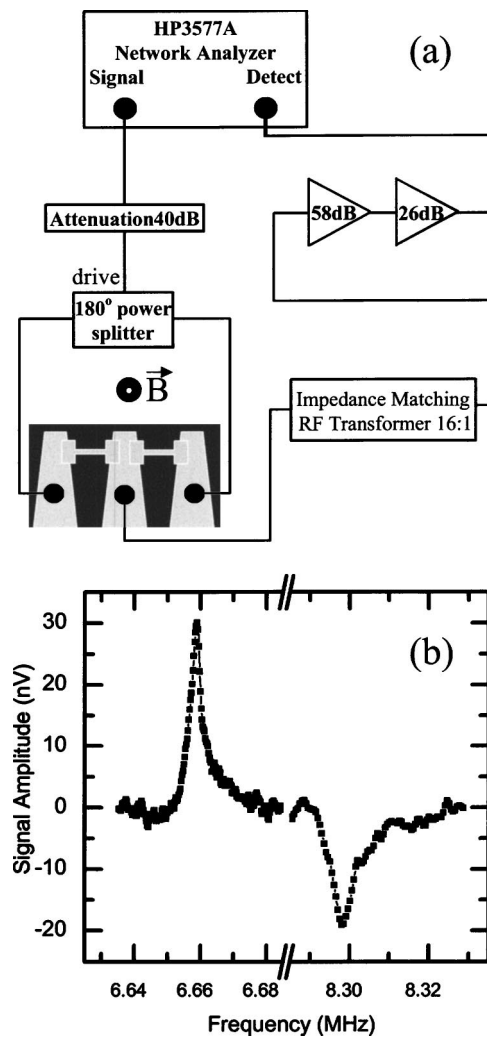


FIG. 2. Schematic detection circuit diagram and measured mechanical resonance.

For the present study, the beams were first measured at the base pressure ($\sim 10^{-7}$ Torr) of the turbopumped vacuum chamber. Small flows of gas were then introduced into the chamber through a needle valve; the pressure was measured with an ion gauge and allowed to stabilize for each data point. The effects of three gases (dry nitrogen, helium, and hydrogen) were studied between 10^{-7} and 10^{-4} Torr. The time required for pressure stabilization in the chamber is on the order of minutes, which dominates the overall response time of the system. This gives an upper limit for the time constant of sensor response.

Figure 3 shows the measured resonance frequency as a function of gas pressure for the three gases studied. For all three gases, the resonant frequency decreases with increasing pressure; the frequency shifts are reversible, and the system returns to its original state upon pumping to the base pressure. For nitrogen and helium, the frequency steadily decreases with increasing pressure over the entire range. Because the frequency of a damped resonator is lower than the natural frequency, one possible explanation for the observed decrease is an increase in damping with increasing pressure. However, the quality factor of the resonator does not measurably change with pressure until $\sim 10^{-2}$ Torr, so it is possible to rule out this effect. Therefore, we believe that surface adsorption of gaseous species is the cause of the observed

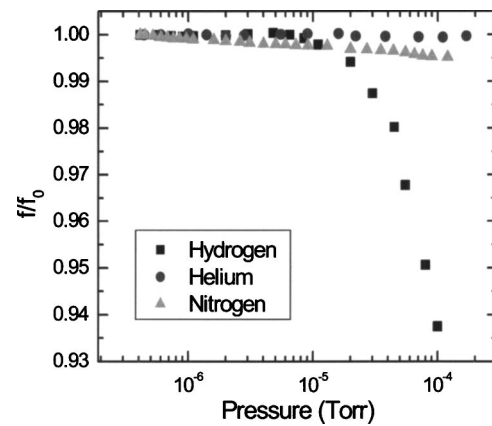


FIG. 3. Frequency shift vs gas pressure, for different gas species.

frequency shift. The larger observed shift associated with nitrogen adsorption is consistent with this mechanism.⁹

The data for hydrogen show dramatic effects that are not present for helium and nitrogen. At low pressures, the frequency decreases very little with increasing pressure, consistent with the small mass of H_2 . Above $\sim 10^{-5}$ Torr, however, the beam's frequency decreases dramatically with increasing pressure, reaching a shift of $\sim 6\%$ at 10^{-4} Torr. A shift of this magnitude cannot be explained by simple adsorption, and as for the other gases, the quality factor does not change over this pressure range.

We attribute the observed frequency shift to a combination of surface absorption mass loading and relief of built-in stress in the metallic components. At low pressure end, the frequency shift can be accounted for by mass loading onto the beam surface.¹⁰ When the hydrogen pressure exceeds about 10^{-5} Torr, the residence time of the hydrogen molecules on the surface is long enough to allow for dissociation into atomic hydrogen. The atomic hydrogen then diffuses into the lattice of the alloy, forming an interstitial phase. The metal lattice then expands and relieves the built-in tensile stress [Fig. 1(b)] in the beams, causing a sharp decrease in the resonant frequency.

The resonant frequency f_0 of a rectangular doubly clamped beam under zero tension is given by

$$f_0 = 1.03 \frac{w}{L^2} \sqrt{\frac{E}{\rho}}, \quad (1)$$

where w is the beam width in the plane of vibration, L is the length, E is the Young's modulus, and ρ is the density. Under stress, the resonant frequency increases according to¹¹

$$f = f_0 \cdot \sqrt{1 + \frac{\sigma L^2}{3.4Ew^2}}, \quad (2)$$

where σ is the tensile stress. For the beam under study, Eq. (1) predicts a resonant frequency of ~ 4 MHz (the exact Young's modulus of the evaporated AuPd alloy is difficult to determine, but should be near 100 GPa). The measured frequency is a factor of 1.5 greater (~ 6 MHz), indicating that the term inside the square root in Eq. (2) is equal to ~ 2.25 , so that the tension and the intrinsic bending stiffness of the beam contribute roughly equally to the frequency.

In a doubly clamped beam, a fractional change $\Delta a/a$ in the zero-tension lattice constant due to hydrogen absorption will change the tension according to

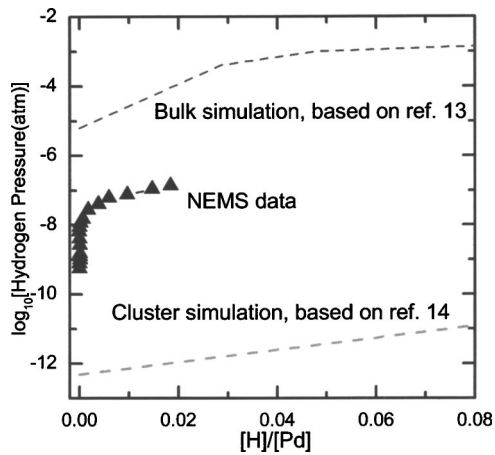


FIG. 4. Comparison with theoretical simulations for bulk Pd (see Ref. 13) and Pd clusters (see Ref. 14).

$$\Delta\sigma = -E \frac{\Delta a}{a}. \quad (3)$$

For small changes in tension, Eqs. (1)–(3) can be combined to yield

$$\frac{\Delta f}{f} \approx -\frac{1}{3.4} \left(\frac{L}{w}\right)^2 \frac{\Delta a}{a}. \quad (4)$$

Equation (4) shows the advantage of using a high aspect ratio nanomechanical device for sensitive detection of small changes in lattice constant: the fractional change in frequency shift is greater than the fractional change in lattice constant by a factor proportional to the square of the aspect ratio. For the beam under study (aspect ratio ~ 80), the fractional frequency shift is greater than the fractional lattice constant shift by a factor of ~ 1880 . This allows us to measure the lattice constant shift very finely: the 6% frequency shift observed at 10^{-4} Torr corresponds to a change in lattice constant of $\sim 3 \times 10^{-5}$. The ultimately resolvable fractional lattice constant change (corresponding to easily resolved frequency shifts of $\sim 0.1\%$) is well below 10^{-6} .

Using Eq. (4), it is possible to compare our measured results to published data for the hydrogen–palladium system. The relationship between the lattice constant and the concentration of interstitial hydrogen in gold–palladium alloy has been studied by x-ray diffraction experiments,¹² which numerically give:

$$\frac{\Delta a}{a} \approx 0.038 \cdot \frac{[H]}{[M]}. \quad (5)$$

Wolf *et al.* have done Monte Carlo simulations of the pressure–composition isotherms for both bulk¹³ and nanocrystalline cluster¹⁴ palladium. To make a qualitative comparison with existing theoretical results, we scale the measured frequency shift by a factor of 0.4 to account for the Pd concentration in the alloy. This comparison plot is shown in Fig. 4. The hydrogen absorption behavior of the NEMS resonator (with an onset of 10^{-5} Torr) is intermediate between the behavior of bulk Pd and Pd clusters. This is to be expected, because the size scale of the beam is intermediate between these two extremes. It is also interesting to note that the NEMS data capture much more of the detailed behavior at low pressures than theory or XRD experiments: NEMS

may offer a unique method to study this phenomenon at ultralow loading.

Finally, we comment briefly on issues related to application of NEMS hydrogen sensors. These initial experiments are done under vacuum conditions. For atmospheric pressure operation, the NEMS device could be operated in a differentially pumped system: our NEMS beams provide good resonant signals up to pressures of ~ 1 Torr. In that case, the onset of absorption at a partial pressure of 10^{-5} Torr would indicate an overall device sensitivity of ~ 10 ppm. Furthermore, differential pumping may not be necessary: it has been demonstrated that it is possible to operate nanomechanical resonators at atmospheric pressure without significantly compromising their apparent quality factor, with the help of parametric amplification.¹⁵ The incorporation of a mechanical parametric amplifier¹⁶ into our system would pose technical challenges, but can be considered a proven technology nonetheless.

These initial experiments have shown that NEMS resonators can be used for highly sensitive, specific gas phase detection. It should be possible to extend this technique to other gas phase systems by employing beams with different composition. NEMS hydrogen sensing also provides a new method for studying the formation of interstitial hydrogen in metals at very low pressures. Better understanding of this phenomenon may potentially lead to new practical applications in the area of hydrogen storage and catalysis.

This work was partially supported by the Nanoscale Science and Engineering Initiative of the National Science Foundation under NSF Award No. CHE-0117752 and by the New York State Office of Science, Technology, and Academic Research (NYSTAR).

¹H. G. Craighead, *Science* **290**, 1532 (2000); M. L. Roukes, *Sci. Am.* **285**, 48 (2001); *Phys. World* **14**, 25 (2001).

²T. Thundat, E. Finot, Z. Hu, R. H. Ritchie, G. Wu, and A. Majumdar, *Appl. Phys. Lett.* **77**, 4061 (2000).

³F. Favier, E. C. Walter, M. P. Zach, T. Benter, and R. M. Penner, *Science* **293**, 2227 (2001).

⁴C. A. Grimes, K. G. Ong, O. K. Varghese, X. P. Yang, G. Mor, M. Paulose, E. C. Dickey, C. M. Ruan, M. V. Pishko, J. W. Kendig, and A. J. Mason, *Sensors* **3**, 69 (2003).

⁵Y. M. Wong, W. P. Kang, J. L. Davidson, A. Wisitsora-at, and K. L. Soh, *Sens. Actuators B* **93**, 327 (2003).

⁶G. J. Kroes, *Prog. Surf. Sci.* **60**, 1 (1999).

⁷A. N. Cleland and M. L. Roukes, *Nature (London)* **392**, 160 (1998); X. M. H. Huang, C. A. Zorman, M. Mehregany, and M. L. Roukes, *ibid.* **421**, 496 (2003).

⁸K. L. Ekinci, Y. T. Yang, X. M. H. Huang, and M. L. Roukes, *Appl. Phys. Lett.* **81**, 2253 (2002).

⁹K. L. Ekinci, Y. T. Yang, and M. L. Roukes, *J. Appl. Phys.* **95**, 2682 (2004).

¹⁰N. V. Lavrik and P. G. Datskos, *Appl. Phys. Lett.* **82**, 2697 (2003); B. Ilic, H. G. Craighead, S. Krylov, W. Senaratne, C. Ober, and P. Neuzil, *J. Appl. Phys.* **95**, 3694 (2004); K. L. Ekinci, X. M. H. Huang, and M. L. Roukes, *Appl. Phys. Lett.* **84**, 4469 (2004).

¹¹A. Bokaian, *J. Sound Vib.* **142**, 481 (1990).

¹²A. Maeland and T. B. Flanagan, *J. Phys. Chem.* **69**, 3575 (1965); Y. Sakamoto, K. Yuwasa, and K. Hirayama, *J. Less-Common Met.* **88**, 115 (1982).

¹³R. J. Wolf, M. W. Lee, R. C. Davis, P. J. Fay, and J. R. Ray, *Phys. Rev. B* **48**, 12415 (1993).

¹⁴R. J. Wolf, M. W. Lee, and J. R. Ray, *Phys. Rev. Lett.* **73**, 557 (1994).

¹⁵L. Sekaric, M. Zalalutdinov, R. B. Bhiladvala, A. T. Zehnder, J. M. Parpia, and H. G. Craighead, *Appl. Phys. Lett.* **81**, 2641 (2002).

¹⁶M. L. Roukes, K. L. Ekinci, Y. T. Yang, X. M. H. Huang, H. X. Tang, D. A. Harrington, J. Casey, and J. L. Arlett, Patent No. WO2004041998-A2; AU2003299484-A1 (2004).